Oxidative Generation of Guanine Radicals by Carbonate Radicals and Their Reactions with Nitrogen Dioxide to Form Site Specific 5-Guanidino-4-nitroimidazole Lesions in Oligodeoxynuc...

ARTICLE *in* CHEMICAL RESEARCH IN TOXICOLOGY · SEPTEMBER 2003

Impact Factor: 3.53 · DOI: 10.1021/tx025578w · Source: PubMed

6 AUTHORS, INCLUDING:

Bh Yun
University of Minnesota Twin Cities
23 PUBLICATIONS **392** CITATIONS
SEE PROFILE

Nicholas E Geacintov
New York University
432 PUBLICATIONS **12,028** CITATIONS
SEE PROFILE

Oxidative Generation of Guanine Radicals by Carbonate Radicals and Their Reactions with Nitrogen Dioxide to Form Site Specific 5-Guanidino-4-nitroimidazole Lesions in Oligodeoxynucleotides

Avrum Joffe, Steven Mock, Byeong Hwa Yun, Alexander Kolbanovskiy, Nicholas E. Geacintov, and Vladimir Shafirovich*

Chemistry Department and Radiation and Solid State Laboratory, 31 Washington Place, New York University, New York, New York 10003-5180

Received July 11, 2002

A simple photochemical approach is described for synthesizing site specific, stable 5-guanidino-4-nitroimidazole (NIm) adducts in single- and double-stranded oligodeoxynucleotides containing single and multiple guanine residues. The DNA sequences employed, 5′-d(ACC CG_1C G^*_2TC CG^*_3C G_4CC) and 5′-d(ACC CG_1C G^*_2TC C), were a portion of exon 5 of the *p53* tumor suppressor gene, including the codons 157 (G^*_2) and 158 (G^*_3) mutation hot spots in the former sequence with four Gs and the codon 157 (G^*_2) mutation hot spot in the latter sequence with two Gs. The nitration of oligodeoxynucleotides was initiated by the selective photodissociation of persulfate anions to sulfate radicals induced by UV laser pulses (308 nm). In aqueous solutions, of bicarbonate and nitrite anions, the sulfate radicals generate carbonate anion radicals and nitrogen dioxide radicals by one electron oxidation of the respective anions. The guanine residue in the oligodeoxynucleotide is oxidized by the carbonate anion radical to form the neutral guanine radical. While the nitrogen dioxide radicals do not react with any of the intact DNA bases, they readily combine with the guanine radicals at either the C8 or the C5 positions. The C8 addition generates the well-known 8-nitroguanine (8-nitro-G) lesions, whereas the C5 attack produces unstable adducts, which rapidly decompose to NIm lesions. The maximum yields of the nitro products (NIm + 8-nitro-G) were typically in the range of 20−40%, depending on the number of guanine residues in the sequence. The ratio of the NIm to 8-nitro-G lesions gradually decreases from 3.4 in the model compound, 2′,3′,5′-tri-*O*-acetylguanosine, to 2.1−2.6 in the single-stranded oligodeoxynucleotides and to 0.8−1.1 in the duplexes. The adduct of the 5′-d(ACC CG_1C G^*_2TC C) oligodeoxynucleotide containing the NIm lesion in codon 157 (G_2) was isolated in HPLC-pure form. The integrity of this adduct was established by a detailed analysis of exonuclease digestion ladders by matrix-assisted laser desorption ionization with time-of-flight detection MS techniques.

Introduction

Oxidative modifications (lesions) of DNA molecules arising from the attack of free radicals, oxidants, ionizing radiation, and other DNA-damaging agents are potentially mutagenic and increase the risk of malignant cell transformation (*1*−*3*). The preferred target of oxidative attack in DNA is guanine, the most easily oxidizable natural nucleobase (*4*). Common lesions include both oxidation (*5*) and nitration (*6*) products of guanine. The nitration of guanine generates two major products, the 8-nitro-G[1] (*7*−*11*) and NIm (*12*, *13*) lesions. The 8-nitro-G lesions are unstable and easily depurinate under physiological conditions with a release of free 8-nitro-G. The NIm lesions are chemically more stable and mutagenic in vitro, although they are poor substrates for removal by formamidopyrimidine DNA *N*-glycosylase, a base excision repair enzyme (*13*). Therefore, NIm adducts may be biologically important, and their structural, biochemical, and biological characteristics are therefore of great interest. While NIm lesions in native DNA or oligodeoxynucleotides can be prepared by reaction with peroxynitrite (*13*), we have devised an alternate and convenient approach (*14*) utilizing the combination reaction of $^{\bullet}NO_2$ with long-lived G(−H)$^{\bullet}$ in DNA (Scheme 1). In this approach, the G(−H)$^{\bullet}$ radicals in DNA are generated by the site selective oxidation of guanine by photochemically generated carbonate radical ions, $CO_3^{\bullet-}$. The combination reaction of G(−H)$^{\bullet}$ with $^{\bullet}NO_2$ occurs via two competitive pathways, involving the addition of $^{\bullet}NO_2$ to C8 resulting in the formation of the 8-nitro-G adduct or to C5 with the formation of an unstable adduct, which spontaneously collapses to the stable NIm adduct.

In this paper, utilizing the photochemical method for generating $CO_3^{\bullet-}$ and $^{\bullet}NO_2$ reactive radical species, we studied the formation of the two types of guanine nitration products (NIm and 8-nitro-G) in single-stranded oligodeoxynucleotide sequences containing only one distinguishable guanine residue. Furthermore, the reactivi-

* To whom the correspondence should be addressed. Tel: (212)998 8456. Fax: (212)998 8421. E-mail: vs5@nyu.edu.

[1] Abbreviations: G(−H)$^{\bullet}$, neutral guanine radical; 8-nitro-G, 8-nitroguanine; NIm, 5-guanidino-4-nitroimidazole; 8-oxo-G, 8-oxo-7,8-dihydroguanine; $CO_3^{\bullet-}$, carbonate radical anion; $^{\bullet}NO_2$, nitrogen dioxide radical; ESI, electrospray ionization; MALDI-TOF, matrix-assisted laser desorption ionization with time-of-flight detection.

10.1021/tx025578w CCC: $25.00
Published on Web 07/11/2003

Scheme 1. Site Selective Nitration of Guanine Bases in DNA by Photochemically Generated $CO_3^{\bullet-}$ and $^{\bullet}NO_2$ Radicals

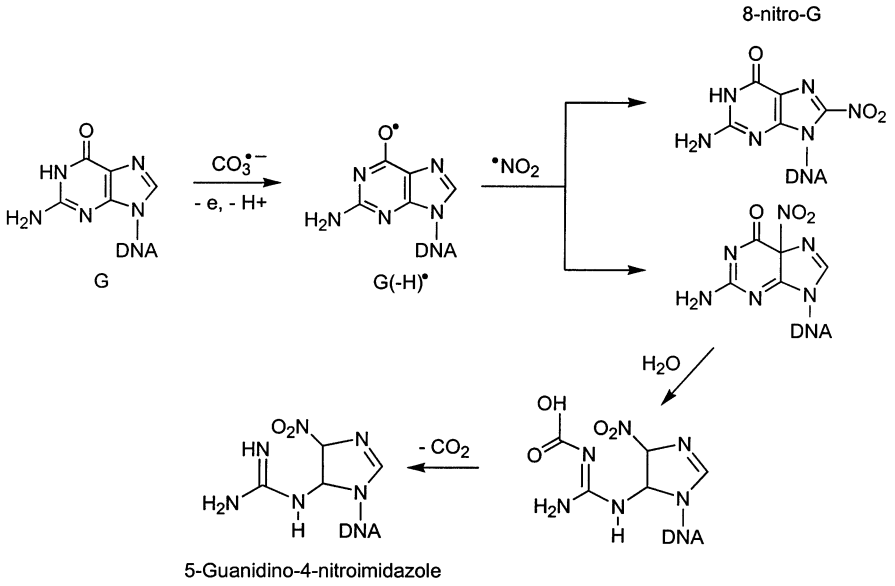

ties of different guanine residues in strands containing two or four guanines were investigated. As an example of a DNA sequence with multiple guanines, we selected a portion of exon 5 of the *p53* tumor-suppressor gene that contains a prominent hot spot observed in smoking-induced lung cancer (*15*, *16*). The sequence **2** is 15 nucleotides long and contains four guanine residues, including the codon 157 (G^*_2) and 158 (G^*_3) mutation hot spots (starred):

5'-d(ACC CG_1C G^*_2TC C) **1**

5'-d(ACC CG_1C G^*_2TC CG^*_3C G_4CC) **2**

Sequence **1** is a truncated form of sequence **2** but contains only two guanines, including the codon 157 (G^*_2) mutation hot spot. The reactivities of these *p53* sequences with reactive carcinogens are of general interest. The G^*_2 and G^*_3 residues are well-known mutation hot spots associated with lung cancer, and Denissenko et al. (*15*, *16*) found that they are also reactivity hot spots for the most tumorigenic diol epoxide metabolite of benzo[*a*]-pyrene. It has been proposed that the prevalence of G → T transversions at these mutation hot spots in lung cancer tissues of tobacco smokers is the mutagenic signature of benzo[*a*]pyrene and related PAH metabolites (*17*). However, Hecht has pointed out that other highly reactive premutagenic components may also react preferentially at such *p53* mutation hot spots thus contributing to the mutagenic spectrum in *p53* from cancerous lung tissues of smokers (*18*). In this work, we selected these biologically significant DNA sequences to study the nitration of guanines by $CO_3^{\bullet-}$ and $^{\bullet}NO_2$ radicals and found that these reactions occurred very efficiently. Utilizing reversed phase HPLC, we isolated the adduct of oligodeoxynucleotide **1** containing the NIm lesion (G^*_2) in codon 157. The integrity of this adduct was established by a detailed analysis of exonuclease digestion ladders by MALDI-TOF MS techniques.

Experimental Procedures

Materials. All inorganic salts (>99% purity) were obtained from Sigma-Aldrich Fine Chemicals and were used as received. The oligodeoxynucleotides were synthesized by standard automated phosphoramidite chemistry techniques. The tritylated oligodeoxynucleotide was removed from the solid support and deprotected with concentrated ammonium hydroxide. The crude oligonuclotide was purified by reversed phase HPLC, detritylated in 80% acetic acid according to standard protocols, and desalted using reversed phase HPLC.

Nitration of Oligodeoxynucleotides by Photochemically Generated $CO_3^{\bullet-}$ and $^{\bullet}NO_2$ Radicals. The detailed protocol of the photochemical radical nitration of the oligodeoxynucleotides has been described earlier (*14*). Briefly, air-equilibrated phosphate buffer solutions (pH 7.5) containing 0.05−0.1 μmol of the oligodeoxynucleotide or 0.25 μmol of 2′,3′,5′-tri-*O*-acetylguanosine, 300 μmol of $NaHCO_3$, 1 μmol of $NaNO_2$, and 25 μmol of $Na_2S_2O_8$ in 1 mL were photoexcited with unfocused light pulses (~15 mJ pulse^{-1} cm^{-2}, 10 pulse s^{-1}) from a 308 nm XeCl excimer laser for fixed periods of time. The nitration of the oligodeoxynucleotide was monitored by the growth of the characteristic absorption band of the nitro products in the 320−450 nm region as a function of increasing irradiation time. Typically, after a 20−40 s irradiation of single-stranded sequences or a 60−90 s irradiation of duplexes, the absorbance of nitro products near 385 nm attained ~60−70% of its maximum value. The nitrated oligodeoxynucleotides thus obtained were subjected to analysis by reversed phase HPLC techniques.

HPLC Isolation, Purification, and Desalting of the Nitration Products. The nitrated oligodeoxynucleotides were isolated, purified, and desalted by reversed phase HPLC techniques using a model L-6200 Intelligent Pump (Hitachi Instruments) and an analytical (250 × 4.6 mm i.d.) Microsorb-MV C18 column (Varian, Inc.). Typically, the HPLC separations were performed employing a 10−19% linear gradient of acetonitrile in 50 mM triethylammonium acetate in water (pH 7) for 60 min at a flow rate of 1 mL/min (detection of nitro products at 385 nm). The HPLC fractions containing NIm adducts were evaporated under vacuum to remove acetonitrile. The NIm adducts were extensively purified on an analytical (250 × 4.6 mm i.d.) Hypersil ODS column (Varian, Walnut Creek, CA) using isocratic mobile phases of acetonitrile and 50 mM triethylammonium acetate, 9:91, for 20 min and then 10:90 for 30 min at flow rates of 1 mL/min. The purified adducts were desalted by reversed phase HPLC employing the following mobile phases: 10 mM ammonium acetate (10 min), deionized water (10 min), and an isocratic 50:50 acetonitrile and H_2O mixture (15 min).

ESI/MS and MALDI-TOF MS Assays of the Reaction Products. MALDI-TOF mass spectra were acquired using a Bruker OmniFLEX instrument. The matrix was a 2:1 mixture of 2′,4′,6′-trihydroxyacetophenone methanol solution (30 mg/mL) and ammonium citrate aqueous solution (100 mg/mL). The aliquots (1−2 μL) of the 10 pmol/μL desalted samples and the matrix solution were spotted on a MALDI target and air-dried before analysis. The mass spectrometer equipped with a 337 nm nitrogen laser was operated in the negative linear mode (accelerating voltage, 19 kV; extraction voltage, 92.7% of the accelerating voltage; ion focus, 9 kV; and delay time, 250 ns). Each spectrum was obtained with an average of 50−100 laser shots.

The ESI mass spectra were acquired using an API I quadrupole mass spectrometer (Perkin-Elmer Sciex Instruments) equipped with an ESI source. The 10 pmol/μL desalted samples in 70:30 MeCN:50 mM imidazole aqueous solution were infused at a 10 μL/min flow rate. The instrument was operated in the negative ion mode; the electrospray voltage was maintained at −4300 V, and the sheath gas pressure was 40 psi. The mass spectra were internally calibrated by using synthetic oligodeoxynucleotides of known molecular weights.

Exonuclease Digestion for Oligodeoxynucleotide Sequencing. Oligodeoxynucleotide samples (150 pmol) were dissolved in 6 μL of water. For digestion from the 3′ end, 6 μL of 100 mM ammonium citrate (pH was adjusted to 9.4 by NH_4OH) and 0.5 μL of snake venom phosphodiesterase (0.004 units/μL) were added to the sample solution. The digest solutions were incubated at 37 °C. For digestion from the 5′ end, 7 μL of water and 1 μL of bovine spleen phosphodiesterase (0.005 units/μL) were added to the sample solution. The digest solutions were kept at room temperature. The aliquots (1 μL) of the digest solutions were removed after fixed periods of time and placed on dry ice to stop the digestion. The aliquots (1−2 μL) of the samples and the trihydroxyacetophenone matrix solution were immediately spotted on a MALDI target and air-dried before analysis.

Results

Generation of NIm Lesions in Single-Stranded DNA. The photochemical nitration based on combination reaction of $^{\bullet}NO_2$ radicals with long-lived G(−H)$^{\bullet}$ radicals in DNA generates both NIm and 8-nitro-G lesions (Scheme 1). The 8-nitro-G adducts prepared by this method were successfully isolated and purified by reversed phase HPLC and characterized by ESI/MS and MALDI-TOF MS techniques (*14*). Here, we focus on isolation, purification, and characterization of the NIm adducts. We begin with single-stranded oligonuclotide 5′-d(CCATCGCTACC) containing a single guanine residue.

A typical reversed phase HPLC elution profile of the irradiated solution (20 s excimer laser irradiation) of 5′-d(CCATCGCTACC) recorded at 385 nm exhibits two prominent fractions containing nitro products (Figure 1A). These products eluted at 15.1 and 23.3 min and were identified as 5-guanindino-4-nitroimidazole and 8-nitro-G adducts, respectively, as reported previously (*14*). After a second HPLC purification of the modified oligonucleotide 5′-d(CCATC[NIm]CTACC), its UV absorption spectrum was determined and a prominent UV absorption maximum at ∼265 nm was observed. The characteristic absorption band at 385 nm is due to the presence of the nitro group (for more details, see Supporting Information). Using the molar absorptivities at 385 nm of the NIm (∼6.5 × 10^3 M^{-1} cm^{-1}) and 8-nitro-G (∼8.4 × 10^3 M^{-1} cm^{-1}) lesions, we calculated that the NIm and 8-nitro-G lesions formed in a ratio of 2.6 (Figure 1). The maximum yields of these lesions (NIm + 8-nitro-G) estimated from the nitration kinetics (data not shown) attain ∼28% (Table 1).

The analogous photochemical nitration of the model compound, 2′,3′,5′-tri-*O*-acetylguanosine in which three sugar hydroxyls are protected from reactions with elec-

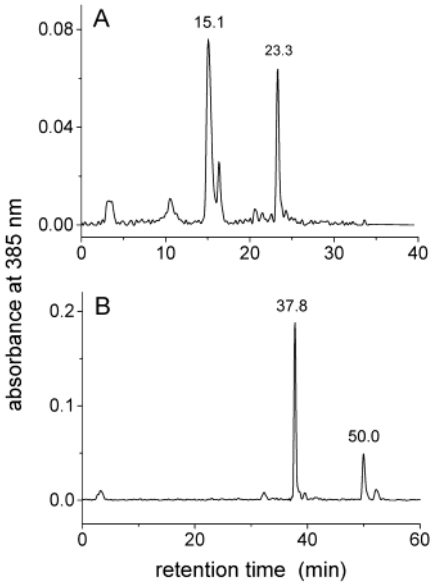

Figure 1. Reversed phase HPLC elution profiles of the single-stranded oligodeoxynucleotide, 5′-d(CCATCGCTACC) (A), and 2′,3′,5′-tri-*O*-acetylguanosine (B) nitrated by the photochemical generation of $CO_3^{\bullet-}$ and $^{\bullet}NO_2$ radicals. Irradiation for 20 s by a pulse train of 308 nm XeCl excimer laser (15 mJ $pulse^{-1}$ cm^{-2}, 10 pulse s^{-1}) of an air-equilibrated 20 mM phosphate buffer solution (pH 7.5) containing 0.1 mM oligodeoxynucleotide or 0.25 mM 2′,3′,5′-tri-*O*-acetylguanosine, 300 mM $NaHCO_3$, 1 mM $NaNO_2$, and 25 mM $Na_2S_2O_8$. HPLC elution conditions: 11−20% linear gradient of acetonitrile in 50 mM triethylammonium acetate (pH 7) for 60 min at a flow rate of 1 mL/min (A); an isocratic mixture of methanol and 50 mM ammonium acetate (5:95) for 10 min, a 5−40% linear gradient of methanol in 50 mM ammonium acetate for 20 min, an isocratic phase of methanol and 50 mM ammonium acetate (40:60) for 12 min, a 40−5% linear gradient of methanol in 50 mM ammonium acetate for 3 min, and an isocratic mixture of methanol and 50 mM ammonium acetate (5:95) for 25 min, all at a flow rate of 1 mL/min (B). The 5′-d(CCATC[NIm]CTACC) and 5′-d(CCATC-[8-nitro-G]CTACC) adducts elute at 15.1 and 23.3 min, respectively (A). The NIm and 8-nitro-G eluted at 37.8 and 50.0 min, respectively (B).

Table 1. Yields of the NIm and 8-Nitro-G Lesions Derived from the Nitration of Guanine Bases in Single- and Double-Stranded Oligodeoxynucleotides and Free Nucleoside by Photochemically Generated $CO_3^{\bullet-}$ and $^{\bullet}NO_2$ Radicals

sequence	*Y*(NIm)[a] (%)	*Y*(8-nitro-G)[a] (%)	Nim/ 8-nitro-G	Y_{max}[b] (%)
5′-CCATCGCTACC	72	28	2.6	28
2′,3′,5′-tri-*O*-acetylguanosine	77	23	3.4	21
5′-ACCCGCGTCC	71	29	2.5	25
5′-ACCCGCGTCCGCGCC	68	32	2.1	37
5′-AACGCGAATTCGCGTT 3′-TTGCGCTTAAGCGCAA	52	48	1.1	38
5′-AACCGGAATTCCGGTT 3′-TTGGCCTTAAGGCCAA	44	56	0.8	37

[a] Relative yields of the NIm, *Y*(NIm), 8-nitro-G, and *Y*(8-nitro-G) lesions were calculated by integration of the HPLC peaks using the molecular absorptivites at 385 nm of the NIm (∼6.5 × 10^3 M^{-1} cm^{-1}) and 8-nitro-G (∼8.4 × 10^3 M^{-1} cm^{-1}) lesions. [b] The maximum yields, Y_{max}, of these lesions (NIm + 8-nitro-G) were estimated from the nitration kinetics recorded at 385 nm.

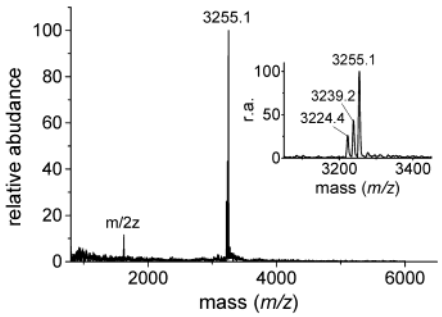

Figure 2. MALDI-TOF negative ion spectrum of the HPLC pure 5′-d(CCATC[NIm]CTACC) adduct.

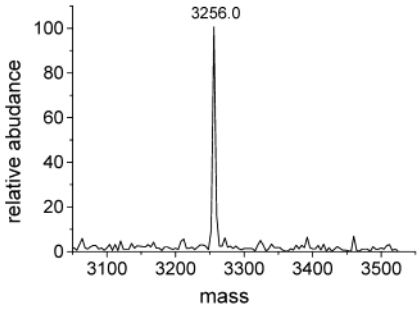

Figure 3. ESI mass spectrum of the HPLC pure oligodeoxynucleotide 5′-d(CCATC[NIm]CTACC) adduct.

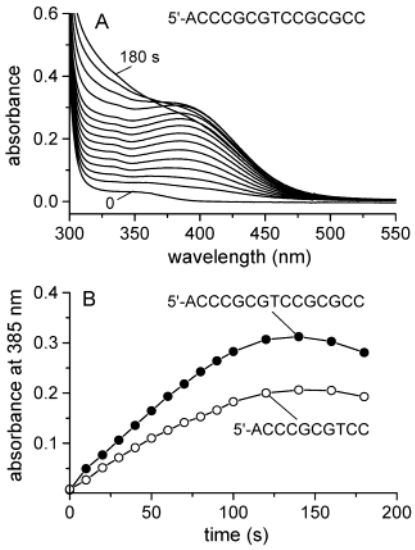

Figure 4. Nitration of the 5′-d(ACCCGCGTCC) and 5′-d(ACCCGCGTCCGCGCC) sequences (0.075 mM) by photochemically generated $CO_3^{\bullet-}$ and $^{\bullet}NO_2$ radicals in an air-equilibrated phosphate buffer solution (pH 7.5) containing 300 mM $NaHCO_3$, 1 mM $NaNO_2$, and 25 mM $Na_2S_2O_8$. (A) Absorption spectra of a reaction mixture containing 5′-d(ACCCGCGTCCGCGCC) measured at various irradiation times after excitation with 308 nm XeCl excimer laser pulses (15 mJ pulse^{-1} cm^{-2}, 10 pulse s^{-1}). (B) Kinetics of photochemical nitration recorded at 385 nm.

trophiles by acetate groups, gave similar results. The acylated nitro products formed with a yield of ∼21% (Table 1) and, because of their enhanced hydrophobic character, were easily separated by reversed phase HPLC (Figure 1B). However, the ratio (3.4) of the NIm and 8-nitro-G nucleosides was somewhat greater than that for the single-stranded sequence (Table 1).

The MALDI-TOF mass spectrum of the 5′-d(CCATC[NIm]CTACC) adduct, recorded in the negative mode, resembles the signals of $[M - H]^-$ ions (Figure 2). This spectrum exhibits a major signal at *m*/*z* 3255.1 and minor signals at *m*/*z* 3239.2 and *m*/*z* 3224.4 as shown in the inset of Figure 2. The former signal is attributed to the NIm adduct (M + 19) with a calculated value of *m*/*z* 3255.2 for the $[M - H]^-$ ion. The minor signals are assigned to the fragmentation products of the 5-guanidino-4-nitrosoimidazole adduct. Fragmentation of the nitro group, induced by the intense UV laser pulses that vaporize the sample in the MALDI-TOF mass spectrometer, results in the formation of a unique series of ions associated with nitroso (*m*/*z* 3239.2, M + 3) and amino (*m*/*z* 3224.4, M − 11) derivatives. Such additional signals have been observed in MALDI-TOF mass spectra of the 8-nitro-G adducts (*14*) and nitrated peptides (*19*, *20*). The fragmentation of the 5-guanidino-4-nitrosoimidazole lesions can depend on the conditions of the matrix-assisted desorption and has not been detected by Gu et al. (*13*) who used a different matrix and instrument.

The integrity of the 5′-d(CCATC[NIm]CTACC) adduct was confirmed by ESI/MS analysis (Figure 3). The 5′-d(CCATC[NIm]CTACC) adduct exhibits a single peak at 3256.0 (calculated molar mass, 3256.2), indicating that the mass of the nitrated oligodeoxynucleotide is 19 amu greater (M + 19) than that of M, the unmodified oligodeoxynucleotide 5′-d(CCATCGCTACC) at 3237.2 (data not shown). These results are consistent with the presence of a NIm lesion in this oligodeoxynucleotide instead of guanine. The nitro group remains intact during the ESI analysis, in agreement with the results of Gu et al. (*13*). The nitro group is also stable during ESI/MS analysis of other nitroderivatives such as 8-nitro-G adducts (*14*) and the 3-nitrotyrosine residues in nitrated peptides (*19*, *21*, *22*).

The NIm lesions are more stable than the 8-nitro-G lesions that undergo facile depurination under physiological conditions (*8*, *10*, *14*). In neutral aqueous solutions (pH 7), the NIm lesions are stable at ambient temperature but slowly decompose at 90 °C (10−15% decomposition after 6 h). In hot alkaline solutions (1 M piperidine, 90 °C), decay of the NIm lesions occurs with the first-order rate constant of (0.9 ± 0.1) h^{-1} (see, for more details, the Supporting Information). These results agree with the observations of Tannenbaum and coworkers (*13*), who showed using gel electrophoresis assays that the NIm lesions are only partially decomposed after the standard hot piperidine treatment (1 M piperidine, for 30 min at 90 °C).

Radical Nitration of the Single-Stranded Sequences with Multiple Guanine Residues. The progress of the photochemical nitration of the single-stranded oligodeoxynucleotides **1** (2G) and **2** (4G) was monitored by measuring the development of the characteristic absorption band of the nitro products in the 320−450 nm region of the spectrum (Figure 4A). The absorbances of the nitro products recorded at 385 nm grow with increasing irradiation time and attain maximum values at ∼2.5 min; further irradiation results in a gradual decomposition of the nitro products (Figure 4B). In the next experiments, we limited irradiation times up to 30−40 s to favor formation of the mononitrated products.

A typical reversed phase HPLC elution profile of the irradiated solution (30 s excimer laser irradiation) of 5′-d(ACCCGCGTCC) recorded at 385 nm exhibits five prominent fractions of the nitro products (Figure 5A). The absorption spectra of these products revealed that the

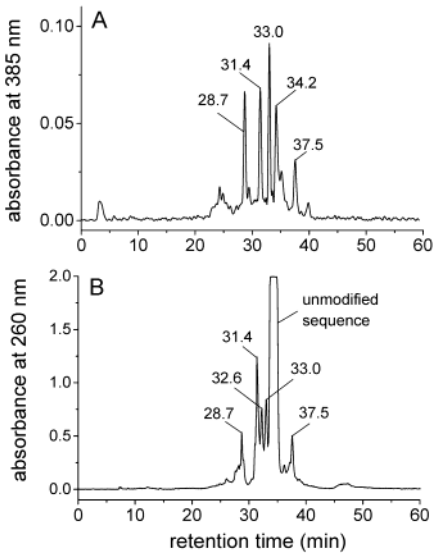

Figure 5. Reversed phase HPLC elution profile of the single-stranded oligodeoxynucleotide, 5′-d(ACCCGCGTCC), nitrated by photochemically generated $CO_3^{\bullet-}$ and $^{\bullet}NO_2$ radicals. Irradiation for 30 s by a pulse train of 308 nm XeCl excimer laser (15 mJ pulse^{-1} cm^{-2}, 10 pulse s^{-1}) of an air-equilibrated 20 mM phosphate buffer solution (pH 7.5) containing 0.1 mM oligodeoxynucleotide, 300 mM $NaHCO_3$, 1 mM $NaNO_2$, and 25 mM $Na_2S_2O_8$. HPLC elution conditions: 10−18% linear gradient of acetonitrile in 50 mM triethylammonium acetate (pH 7) for 60 min at a flow rate of 1 mL/min. The double NIm adduct eluted at 28.7, the mono-NIm adducts eluted at 31.4 and 34.2 min, and the mono-8-nitro-G adducts eluted at 33.0 and 37.5 min. A sequence with an abasic site that has no absorbance at 385 nm and does not manifest itself in panel A elutes at 32.6 min as shown in panel B (see the text for more details).

fractions eluting at 28.7, 31.4, and 34.2 min are the NIm adducts (λ_{max} = 385 nm) and those eluted at 33.0 and 37.5 min are the 8-nitro-G adducts (λ_{max} = 400 nm). In agreement with these assignments, the MALDI-TOF mass spectra of these nitro products showed that the product eluted at 28.7 min is the double 5-guanindino-4-nitroimidazole adduct (*m*/*z* 2986.6, M + 38), the products eluting at 31.4 and 34.2 min are the mono-5-guanindino-4-nitroimidazole adduct (*m*/*z* 2967.3, M + 19), and those eluted at 33.0 and 37.5 min are the mono-8-nitro-G adducts (*m*/*z* 2993.4, M + 45). Another reaction product, detectable by its absorbance at 260 nm (Figure 5B) but not absorbing at 385 nm (Figure 5A), eluted at 32.6 min. The mass of this product (*m*/*z* 3101.9, M − 133) is consistent with the mass of the oligonucleotide with an abasic sequence 5′-d(CCATC_CTACC) missing the guanine base moiety.

The reversed phase HPLC elution profile of the irradiated solution of 5′-d(ACCCGCGTCCGCGCC) recorded at 385 nm was more complex and exhibited eight partially resolved peaks arising from the 5-guanindino-4-nitroimidazole and 8-nitro-G adducts (see, for more details, the Supporting Information). Using the molar absorbtivities of the 5-guanindino-4-nitroimidazole and 8-nitro-G lesions, we estimated that the NIm and 8-nitro-G lesions formed in approximately the same ratios as in the case of sequence with single G (Table 1).

In the next experiments, we focused on the mono-5-guanindino-4-nitroimidazole adduct of sequence **1** eluting at 31.4 min because this product and the unmodified sequence are clearly resolved even in the gradient regime (Figure 5B). This adduct was extensively purified by several reversed phase HPLC runs to remove contamination of the spiroiminodihydantoin adduct (*23*, *24*), which is the major end product of guanine oxidation by $CO_3^{\bullet-}$ radicals (*25*). The MALDI-TOF instrument response in the case of the spiroiminodihydantoin adduct was higher than in the case of the 5-guanindino-4-nitroimidazole adduct, and the residual signal of this adduct is clearly observed as a minor signal at *m*/*z* 2980.5 (M + 32) even after extensive purification of the sample (Figures 6 and 7).

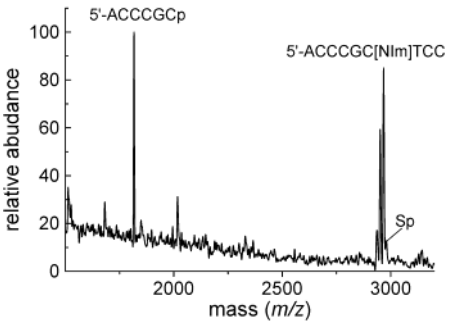

Figure 6. MALDI-TOF negative ion spectra of the 5′-d(ACCCGC[NIm]TCC) adduct after treatment with hot piperidine at 90 °C for 2 h.

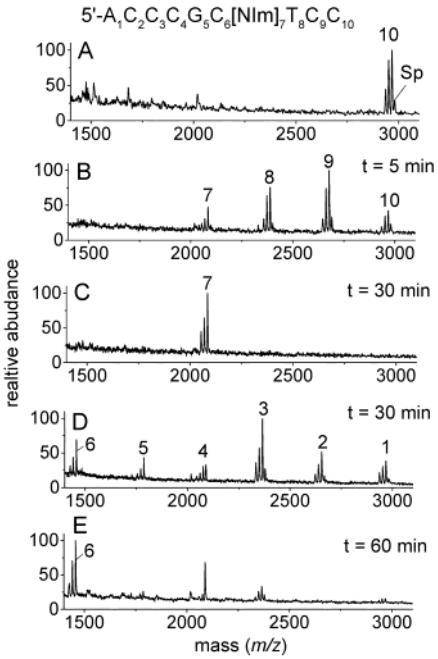

Figure 7. Time-dependent MALDI-TOF mass spectra of the 5′-d(ACCCGC[NIm]TCC) adduct digested by snake venom phosphodiesterase (B and C) and by bovine spleen phosphodiesterse (D and E) after fixed periods of time. Panel A shows the initial spectrum of the pure adduct.

The position of 5-guanindino-4-nitroimidazole lesion in the mononitrated adduct of 5′-d(ACCCGCGTCC) sequence eluting at 31.4 min (Figure 5) was established by the MALDI-TOF MS analysis of the adduct treated by hot piperidine at 90 °C (*26*). Typically, this treatment of alkali-labile lesions induces β,δ-elimination leading to DNA fragments containing 5′- and 3′-phosphate termini (*27*). The MALDI-TOF mass spectrum of the adduct treated by hot piperidine for 2 h shows three signals at *m*/*z* 2967.1, 2951.5, and 2936.0 related to starting mono-5-guanindino-4-nitroimidazole adduct and a new signal at *m*/*z* 1816.7 (Figure 6). The latter signal at *m*/*z* 1816.7 was assigned to 5′-ACCCGCp sequence arising from the cleavage of the 5′-d(ACCCGC[NIm]TCC) adduct (the

short fragment, 5′-pTCC, cannot be clearly detected due to interference with matrix signals). The signals related to cleavage products of the 5′-d(ACCC[NIm]CGTCC) adduct (5′-ACCCp and 5′-pCGTCC) are not observed. Thus, the 5-guanindino-4-nitroimidazole adduct eluting at 31.4 min is mostly 5′-d(ACCCGC[NIm]TCC).

The integrity of the 5′-d(ACCCGC[NIm]TCC) adduct was confirmed by the exonuclease digestion ladders obtained by MALDI-TOF MS techniques (*28*). The stepwise digestion of the adducts starting from the 3′ end was performed by snake venom phosphodiesterase; the adducts were digested by bovine spleen phosphodiesterase beginning from the 5′ end. Typical time-dependent MALDI-TOF mass spectra of 5′-d(ACCCGC[NIm]TCC) recorded in the negative mode are shown in Figure 7. The signal of the pure adduct is shown in panel A. The stepwise digestion of the adduct by snake venom phosphodiesterase induces release of the first three nucleotides from the 3′ end (panel B). However, this enzyme is unable to cleave the phophodiester bond between the 5-guanindino-4-nitroimidazole and the 3′-cytidine base and the signal at *m*/*z* 2084.5 related to 5′-d(ACCCGC-[NIm]) is detected even after a prolonged incubation (panel C). Further experiments showed that snake venom phosphodiesterase was unable to bypass the 5′-C-[NIm]-3′ site even at higher enzyme concentrations or upon prolonged incubation. The bovine spleen phosphodiesterase clearly cut off only the first five nucleotides from the 5′ end (panel D), and the signal at *m*/*z* 1457.6 related to 5′-d(C[NIm]TCC) sequence is observed after a long incubation time (panel E). The shorter fragments were not detected due to interference from matrix signals. Thus, it was difficult to determine whether bovine spleen phosphodiesterase stops at the 5′-cytidine base before the nitroimidazole or is able to bypass the 5′-C-[NIm]-3′ site at higher enzyme concentrations or prolonged incubation. This high resistance to exonuclease digestion has been recently reported for the processing of the site-specifically modified 5-hydroxy-5-methylhydantoin oligodeoxynucleotides (*29*).

Effects of DNA Secondary Structure on the Relative Yields of the Nitro Products. To reach a better understanding of the role of secondary DNA structure on the formation of the 5-guanindino-4-nitroimidazole and 8-nitro-G lesions, we explored the radical nitration reactions of guanines in double-stranded oligodeoxynucleotides. However, the nitration of the duplexes containing single G residue (e.g., the self-complementary 5′-TATAACGTTATA duplex) typically resulted in lower yields of the nitro products in comparison to those obtained in the case of the single-stranded oligonucleotide 5′-d(CCATCGCTACC). To study the nitration reaction yields in double-stranded sequences that contain more than one guanine residue, we used the duplexes formed by the self-complementary sequences 5′-d(AACGCGAATTCGCGT) and 5′-d(AACCGGAATTCCGGTT). These duplexes exhibited well-defined cooperative melting curves with melting temperatures of 66−68 °C (*30*), and the double-stranded forms dominate at room temperature. Because of the presence of multiple G residues in each duplex, the overall nitration yields were improved (Table 1). However, the isolation of the individual 5-guanindino-4-nitroimidazole and 8-nitro-G adducts was necessarily limited due to formation of multiple adducts, and their separation by reversed phase HPLC techniques proved difficult because of the formation of secondary structures in these guanine-rich sequences (*31*, *32*). Nevertheless, we were able to estimate the ratio of the 5-guanindino-4-nitroimidazole and 8-nitro-G lesions formed. The nitro products were isolated from the irradiated solutions of the unmodified duplexes by reversed phase HPLC. After acetonitrile was removed under vacuum, the fractions of the nitro products were incubated at 90 °C for 5 min. This treatment induces the complete depurination of the 8-nitro-G adducts (*10*). The ratio of 8-nitro-G released from the parent adducts and the 5-guanindino-4-nitroimidazole adducts remaining intact in the oligonucleotides can be easily determined from the reversed phase HPLC profiles. The results of these experiments, summarized in Table 1, show that the ratios (0.8−1.1) of the 5-guanindino-4-nitroimidazole to 8-nitro-G lesions generated by nitration of DNA of the duplexes are lower than those in the single-stranded oligodeoxynucleotides.

Discussion

The endogenous nitration of proteins, DNA, and other biomolecules constitutes an important pathway of damage of biomolecules in vivo (*2*, *3*, *33*). In cellular environments, the $^{\bullet}NO_2$ radicals are strong oxidizing agents that are introduced by various mechanisms, including the oxidation of NO_2^- anions by hydrogen peroxide catalyzed by mammalian peroxidases (*34*−*38*), tobacco smoke (*39*, *40*), combustion engine exhaust (*41*), and the reaction of peroxynitrite with carbon dioxide (*42*−*45*). However, the role of $^{\bullet}NO_2$ radicals in potentiating oxidative DNA damage has received relatively little attention due to the known low reactivity of $^{\bullet}NO_2$ radicals with native DNA (*46*). In agreement with predictions based on thermodynamics, $^{\bullet}NO_2$ radicals with a reduction potential, $E°(^{\bullet}NO_2/NO_2^-) = 1.04$ V vs NHE (*47*) do not exhibit observable reactivities toward the four natural DNA bases (A, C, G, and T) but do oxidize 8-oxo-dG (*48*). Thus, oxidants more powerful than the $^{\bullet}NO_2$ radical must first abstract an electron from guanine in DNA in order to allow for a subsequent reaction with $^{\bullet}NO_2$ as outlined in this work. The seemingly best candidate for this primary role in a cellular environment is $CO_3^{\bullet-}$, one of the important free radicals in biological systems (*49*) that can be generated in vivo together with $^{\bullet}NO_2$ radicals via the reaction of peroxynitrite with carbon dioxide (*42*−*45*). The oxidation of the G bases by the $CO_3^{\bullet-}$ radicals is thermodynamically feasible because the reduction potential of the $CO_3^{\bullet-}$ radical at pH 7, $E_7 \sim 1.7$ V vs NHE (*30*), is greater than $E_7 = 1.29$ V vs NHE for G(−H)$^{\bullet}$ radicals (*4*). The generation of $CO_3^{\bullet-}$ in vivo can occur via multiple pathways including one electron oxidation of bicarbonate anions at an active site of copper−zinc superoxide dismutase (*50*−*52*) and the reaction of peroxynitrite with carbon dioxide (*42*−*45*).

Recently, we have investigated the reactions of the $CO_3^{\bullet-}$ radicals with double-stranded DNA by laser flash photolysis techniques (*30*). In the presence of DNA, the $CO_3^{\bullet-}$ radicals induce site selective oxidation of guanine residues monitored by the rise of the characteristic transient absorption band of guanine neutral radicals, G(−H)$^{\bullet}$. Trapping of the long-lived G(−H)$^{\bullet}$ radicals in DNA by $^{\bullet}NO_2$ radicals generates two major end products, the 8-nitro-G and the NIm lesions (*14*). The formation of these lesions occurs by the combination reaction of G(−H)$^{\bullet}$ with $^{\bullet}NO_2$ via two competitive pathways involving the addition of $^{\bullet}NO_2$ to C8 with the formation of the

8-nitro-dG adduct or to C5 with the formation of an unstable adduct, which spontaneously collapses to the stable NIm adduct (Scheme 1).

Here, we explored the nitration of single- and double-stranded DNA containing single and multiple guanine residues in the sequence utilizing the photochemical method for generating the reactive radical species (*14*). In this method, the nitration is triggered by the selective photodissociation of persulfate anions to sulfate radicals induced by UV excitation. While we employed 308 nm laser excitation in this work, photoexcitation using continuous excitation from suitably filtered Hg−Xe or Xe arc lamps (290−340 nm) can also be used for generating the same radical species (*14*). The $CO_3^{\bullet-}$ and $^{\bullet}NO_2$ radicals derived from the one electron oxidation of the HCO_3^- and NO_2^- anions by sulfate radicals induce the efficient nitration of guanine residues in nucleosides and in single- and double-stranded oligonucleotides. In all cases, we found that both the NIm and the 8-nitro-G lesions are formed. The ratio of the NIm and 8-nitro-G lesions gradually decreases from 3.4 in the model compound, 2′,3′,5′-tri-*O*-acetylguanosine, 2.1−2.6 in the single-stranded oligodeoxynucleotides, to 1 in the duplexes (Table 1). This effect of secondary DNA structure on the ratios of these lesions is not surprising since the probability of addition of even the relatively small $^{\bullet}NO_2$ radical to either the C5 or the C8 positions of the G(−H)$^{\bullet}$ radical (accessible from the major groove in double-stranded B-form DNA) can differ from that in single-stranded sequences and in free nucleosides.

The radical nitration of guanines in the codon 157 *p53* model sequences studied occurs efficiently, and NIm lesions are formed. Analysis of the mutation spectra of the *p53* tumor-suppressor gene showed that codons 157 (G^*_1) and 158 (G_3) are common mutation hot spots in lung cancers (mostly G to T transversions) and is much less frequently mutated in breast, colon, and brain cancers (*53*). The nitration of guanines in native double-stranded DNA, including *p53* sequences, as well as the mutagenic potentials of these lesions, are of potential biological interest and should be investigated.

Conclusions

Employing a relatively simple photochemical approach for generation of $CO_3^{\bullet-}$ and $^{\bullet}NO_2$ reactive radical species, we have shown that HPLC-pure oligodeoxynucleotides with a single, site specific NIm lesion can be easily synthesized in quantities of ∼10 nmol, together with the well-established 8-nitro-dG adducts. Structural information on the NIm adducts, as well as on its stability at different temperatures, has been obtained by HPLC methods and combined with ESI and MALDI-TOF mass spectroscopic techniques.

Acknowledgment. This work has been supported by the National Institutes of Health, Grant 1-R01-ES11598-01, and by a grant from the Kresge Foundation.

Supporting Information Available: Absorption spectrum of the NIm adduct, stability of the NIm adduct in neutral and alkaline solutions at 90 °C, reversed phase HPLC elution profile of the single-stranded oligodeoxynucleotide, 5′-d(ACCCGCGTCCGCGCC) nitrated by photochemically generating $CO_3^{\bullet-}$ and $^{\bullet}NO_2$ radicals, the MALDI-TOF negative ion spectra of the mono-NIm adducts prepared by the photochemical nitration of the 5′-d(ACCCGCGTCCGCGCC) sequence. This material is available free of charge via the Internet at http://pubs.acs.org.

References

(1) Beckman, K. B., and Ames, B. N. (1997) Oxidative decay of DNA. *J. Biol. Chem.* **272**, 19633−19636.
(2) Halliwell, B. (1999) Oxygen and nitrogen are pro-carcinogens. Damage to DNA by reactive oxygen, chlorine and nitrogen species: measurement, mechanism and the effects of nutrition. *Mutat. Res.* **443**, 37−52.
(3) Grisham, M. B., Jourd'heuil, D., and Wink, D. A. (2000) Review article: chronic inflammation and reactive oxygen and nitrogen metabolism−implications in DNA damage and mutagenesis. *Aliment. Pharmacol. Ther.* **14** (Suppl. 1), 3−9.
(4) Steenken, S., and Jovanovic, S. V. (1997) How easily oxidizable is DNA? One-electron reduction potentials of adenosine and guanosine radicals in aqueous solution. *J. Am. Chem. Soc.* **119**, 617−618.
(5) Cadet, J., Bellon, S., Berger, M., Bourdat, A. G., Douki, T., Duarte, V., Frelon, S., Gasparutto, D., Muller, E., Ravanat, J. L., and Sauvaigo, S. (2002) Recent aspects of oxidative DNA damage: guanine lesions, measurement and substrate specificity of DNA repair glycosylases. *Biol. Chem.* **383**, 933−943.
(6) Burney, S., Caulfield, J. L., Niles, J. C., Wishnok, J. S., and Tannenbaum, S. R. (1999) The chemistry of DNA damage from nitric oxide and peroxynitrite. *Mutat. Res.* **424**, 37−49.
(7) Yermilov, V., Rubio, J., Becchi, M., Friesen, M. D., Pignatelli, B., and Ohshima, H. (1995) Formation of 8-nitroguanine by the reaction of guanine with peroxynitrite in vitro. *Carcinogenesis* **16**, 2045−2050.
(8) Yermilov, V., Rubio, J., and Ohshima, H. (1995) Formation of 8-nitroguanine in DNA treated with peroxynitrite in vitro and its rapid removal from DNA by depurination. *FEBS Lett.* **376**, 207−210.
(9) Yermilov, V., Yoshie, Y., Rubio, J., and Ohshima, H. (1996) Effects of carbon dioxide/bicarbonate on induction of DNA single-strand breaks and formation of 8-nitroguanine, 8-oxoguanine and base-propenal mediated by peroxynitrite. *FEBS Lett.* **399**, 67−70.
(10) Tretyakova, N. Y., Burney, S., Pamir, B., Wishnok, J. S., Dedon, P. C., Wogan, G. N., and Tannenbaum, S. R. (2000) Peroxynitrite-induced DNA damage in the supF gene: correlation with the mutational spectrum. *Mutat. Res.* **447**, 287−303.
(11) Lee, J. M., Niles, J. C., Wishnok, J. S., and Tannenbaum, S. R. (2002) Peroxynitrite Reacts with 8-Nitropurines to Yield 8-Oxopurines. *Chem. Res. Toxicol.* **15**, 7−14.
(12) Niles, J. C., Wishnok, J. S., and Tannenbaum, S. R. (2001) A Novel Nitroimidazole Compound Formed during the Reaction of Peroxynitrite with 2′,3′,5′-Tri-O-Acetyl-Guanosine. *J. Am. Chem. Soc.* **123**, 12147−12151.
(13) Gu, F., Stillwell, W. G., Wishnok, J. S., Shallop, A. J., Jones, R. A., and Tannenbaum, S. R. (2002) Peroxynitrite-Induced Reactions of Synthetic Oligo 2′-Deoxynucleotides and DNA Containing Guanine: Formation and Stability of a 5-Guanidino-4-nitroimidazole Lesion. *Biochemistry* **41**, 7508−7518.
(14) Shafirovich, V., Mock, S., Kolbanovskiy, A., and Geacintov, N. E. (2002) Photochemically catalyzed generation of site-specific 8-nitroguanine adducts in DNA by the reaction of long-lived neutral guanine radicals with nitrogen dioxide. *Chem. Res. Toxicol.* **15**, 591−597.
(15) Denissenko, M. F., Pao, A., Tang, M., and Pfeifer, G. P. (1996) Preferential formation of benzo[*a*]pyrene adducts at lung cancer mutational hotspots in P53. *Science* **274**, 430−432.
(16) Denissenko, M. F., Chen, J. X., Tang, M. S., and Pfeifer, G. P. (1997) Cytosine methylation determines hot spots of DNA damage in the human P53 gene. *Proc. Natl. Acad. Sci. U.S.A.* **94**, 3893−3898.
(17) Hainaut, P., Olivier, M., and Pfeifer, G. P. (2001) TP53 mutation spectrum in lung cancers and mutagenic signature of components of tobacco smoke: lessons from the IARC TP53 mutation database. *Mutagenesis* **16**, 551−553; author reply 555−556.
(18) Hecht, S. S. (1999) Tobacco smoke carcinogens and lung cancer. *J. Natl. Cancer Inst.* **91**, 1194−1210.
(19) Petersson, A.-S., Steen, H., Kalume, D. E., Caidahl, K., and Roepstorff, P. (2001) Investigation of tyrosine nitration in proteins by mass spectrometry. *J. Mass Spectrom.* **36**, 616−625.
(20) Sarver, A., Scheffler, N. K., Shetlar, M. D., and Gibson, B. W. (2001) Analysis of peptides and proteins containing nitrotyrosine by matrix-assisted laser desorption/ionization mass spectrometry. *J. Am. Soc. Mass Spectrom.* **12**, 439−448.
(21) Yi, D., Smythe, G. A., Blount, B. C., and Duncan, M. W. (1997) Peroxynitrite-mediated nitration of peptides: characterization of

the products by electrospray and combined gas chromatography−mass spectrometry. *Arch. Biochem. Biophys.* **344**, 253−259.
(22) MacMillan-Crow, L. A., Crow, J. P., and Thompson, J. A. (1998) Peroxynitrite-mediated inactivation of manganese superoxide dismutase involves nitration and oxidation of critical tyrosine residues. *Biochemistry* **37**, 1613−1622.
(23) Leipold, M. D., Muller, J. G., Burrows, C. J., and David, S. S. (2000) Removal of hydantoin products of 8-oxoguanine oxidation by the *Escherichia coli* DNA repair enzyme, FPG. *Biochemistry* **39**, 14984−14992.
(24) Kornyushyna, O., Berges, A. M., Muller, J. G., and Burrows, C. J. (2002) In Vitro Nucleotide Misinsertion Opposite the Oxidized Guanosine Lesions Spiroiminodihydantoin and Guanidinohydantoin and DNA Synthesis Past the Lesions Using *Escherichia coli* DNA Polymerase I (Klenow Fragment). *Biochemistry* **41**, 15304−15314.
(25) Joffe, A., Geacintov, N. E., and Shafirovich, V. DNA Lesions Derived from the Site-Selective Oxidation of Guanine by Carbonate Radical Anions. *Chem. Res. Toxicol.*, submitted for publication.
(26) Tretyakova, N. Y., Wishnok, J. S., and Tannenbaum, S. R. (2000) Peroxynitrite-induced secondary oxidative lesions at guanine nucleobases: Chemical stability and recognition by the Fpg DNA repair enzyme. *Chem. Res. Toxicol.* **13**, 658−664.
(27) Burrows, C. J., and Muller, J. G. (1998) Oxidative nucleobase modifications leading to strand scission. *Chem. Rev.* **98**, 1109−1151.
(28) Pieles, U., Zurcher, W., Schar, M., and Moser, H. E. (1993) Matrix-assisted laser desorption ionization time-of-flight mass spectrometry: a powerful tool for the mass and sequence analysis of natural and modified oligonucleotides. *Nucleic Acids Res.* **21**, 3191−3196.
(29) Gasparutto, D., Bourdat, A. G., D'Ham, C., Duarte, V., Romieu, A., and Cadet, J. (2000) Repair and replication of oxidized DNA bases using modified oligodeoxyribonucleotides. *Biochimie* **82**, 19−24.
(30) Shafirovich, V., Dourandin, A., Huang, W., and Geacintov, N. E. (2001) Carbonate radical is a site-selective oxidizing agent of guanines in double-stranded oligonucleotides. *J Biol. Chem.* **276**, 24621−24626.
(31) Germann, M. W., Pon, R. T., and van de Sande, J. H. (1987) A general method for the purification of synthetic oligodeoxyribonucleotides containing strong secondary structure by reversed-phase high-performance liquid chromatography on PRP-1 resin. *Anal. Biochem.* **165**, 399−405.
(32) Arghavani, M. B., and Romano, L. J. (1995) A method for the purification of oligonucleotides containing strong intra- or intermolecular interactions by reversed-phase high-performance liquid chromatography. *Anal. Biochem.* **231**, 201−209.
(33) Ischiropoulos, H., and Beckman, J. S. (2003) Oxidative stress and nitration in neurodegeneration: cause, effect, or association? *J. Clin. Invest.* **111**, 163−169.
(34) Eiserich, J. P., Cross, C. E., Jones, A. D., Halliwell, B., and van der Vliet, A. (1996) Formation of nitrating and chlorinating species by reaction of nitrite with hypochlorous acid. A novel mechanism for nitric oxide-mediated protein modification. *J. Biol. Chem.* **271**, 19199−19208.
(35) Van der Vliet, A., Eiserich, J. P., Halliwell, B., and Cross, C. E. (1997) Formation of reactive nitrogen species during peroxidase-catalyzed oxidation of nitrite. A potential additional mechanism of nitric oxide- dependent toxicity. *J. Biol. Chem.* **272**, 7617−7625.
(36) Eiserich, J. P., Hristova, M., Cross, C. E., Jones, A. D., Freeman, B. A., Halliwell, B., and van der Vliet, A. (1998) Formation of nitric oxide-derived inflammatory oxidants by myeloperoxidase in neutrophils. *Nature* **391**, 393−397.
(37) Sampson, J. B., Ye, Y., Rosen, H., and Beckman, J. S. (1998) Myeloperoxidase and horseradish peroxidase catalyze tyrosine nitration in proteins from nitrite and hydrogen peroxide. *Arch. Biochem. Biophys.* **356**, 207−213.
(38) Byun, J., Henderson, J. P., Mueller, D. M., and Heinecke, J. W. (1999) 8-Nitro-2′-deoxyguanosine, a specific marker of oxidation by reactive nitrogen species, is generated by the myeloperoxidase-hydrogen peroxide- nitrite system of activated human phagocytes. *Biochemistry* **38**, 2590−2600.
(39) Cueto, R., and Pryor, W. A. (1994) Cigarette smoke chemistry: conversion of nitric oxide to nitrogen dioxide and reactions of nitrogen oxides with other smoke components as studied by Fourier transform infrared spectroscopy. *Vib. Spectrosc.* **7**, 97−111.
(40) Hoffmann, D., Hoffmann, I., and El-Bayoumy, K. (2001) The less harmful cigarette: a controversial issue. a tribute to Ernst L. Wynder. *Chem. Res. Toxicol.* **14**, 767−790.
(41) Ohyama, K., Ito, T., and Kanisawa, M. (1999) The roles of diesel exhaust particle extracts and the promotive effects of NO_2 and/or SO_2 exposure on rat lung tumorigenesis. *Cancer Lett.* **139**, 189−197.
(42) Lymar, S. V., and Hurst, J. K. (1995) Rapid reaction between peroxonitrite ion and carbon dioxide: Implications for biological activity. *J. Am. Chem. Soc.* **117**, 8867−8868.
(43) Lymar, S. V., and Hurst, J. K. (1998) CO_2−Catalyzed One-Electron Oxidations by Peroxynitrite: Properties of the Reactive Intermediate. *J. Am. Chem. Soc.* **37**, 294−301.
(44) Bonini, M. G., Radi, R., Ferrer-Sueta, G., Ferreira, A. M., and Augusto, O. (1999) Direct EPR detection of the carbonate radical anion produced from peroxynitrite and carbon dioxide. *J. Biol. Chem.* **274**, 10802−10806; (1999) Published Erratum. *J. Biol. Chem.* **274** (27), 19508.
(45) Squadrito, G. L., and Pryor, W. A. (2002) Mapping the reaction of peroxynitrite with CO_2: energetics, reactive species, and biological implications. *Chem. Res. Toxicol.* **15**, 885−895.
(46) Prütz, W. A., Monig, H., Butler, J., and Land, E. J. (1985) Reactions of nitrogen dioxide in aqueous model systems: oxidation of tyrosine units in peptides and proteins. *Arch. Biochem. Biophys.* **243**, 125−134.
(47) Stanbury, D. M. (1989) Reduction potentials involving inorganic free radicals in aqueous solution. *Adv. Inorg. Chem.* **33**, 69−138.
(48) Shafirovich, V., Cadet, J., Gasparutto, D., Dourandin, A., and Geacintov, N. E. (2001) Nitrogen dioxide as an oxidizing agent of 8-oxo-7,8-dihydro-2′-deoxyguanosine but not of 2′-deoxyguanosine. *Chem. Res. Toxicol.* **14**, 233−241.
(49) Augusto, O., Bonini, M. G., Amanso, A. M., Linares, E., Santos, C. C., and De Menezes, S. L. (2002) Nitrogen dioxide and carbonate radical anion: two emerging radicals in biology. *Free Radical Biol. Med.* **32**, 841−859.
(50) Goss, S. P., Singh, R. J., and Kalyanaraman, B. (1999) Bicarbonate enhances the peroxidase activity of Cu, Zn-superoxide dismutase. Role of carbonate anion radical. *J. Biol. Chem.* **274**, 28233−28239.
(51) Zhang, H., Joseph, J., Felix, C., and Kalyanaraman, B. (2000) Bicarbonate enhances the hydroxylation, nitration, and peroxidation reactions catalyzed by copper, zinc superoxide dismutase. Intermediacy of carbonate anion radical. *J. Biol. Chem.* **275**, 14038−14045.
(52) Zhang, H., Joseph, J., Gurney, M., Becker, D., and Kalyanaraman, B. (2002) Bicarbonate enhances peroxidase activity of Cu, Zn-superoxide dismutase. Role of carbonate anion radical and scavenging of carbonate anion radical by metalloporphyrin antioxidant enzyme mimetics. *J. Biol. Chem.* **277**, 1013−1020.
(53) Pfeifer, G. P., Denissenko, M. F., Olivier, M., Tretyakova, N., Hecht, S. S., and Hainaut, P. (2002) Tobacco smoke carcinogens, DNA damage and p53 mutations in smoking-associated cancers. *Oncogene* **21**, 7435−7451.

TX025578W